

Investigation of Pretreated Switchgrass, Corn Stover, and Hardwood Fuels in Direct Carbon Fuel Cells

Borja Cantero-Tubilla², Katarzyna Sabolsky¹, Edward M. Sabolsky¹, and John W. Zondlo^{2,*}

¹Department of Mechanical and Aerospace Engineering, West Virginia University, Morgantown, WV, 26506, USA

²Department of Chemical Engineering, West Virginia University, Morgantown, WV, 26506, USA

*E-mail: John.zondlo@mail.wvu.edu

Received: 20 August 2015 / Accepted: 5 November 2015 / Published: 1 December 2015

A variety of fuels were evaluated in an electrolyte-supported Direct Carbon Fuel Cell (DCFC). These cells consisted of a planar, 8 mol% Y_2O_3 - ZrO_2 (YSZ) electrolyte with a multilayer $(La_{0.6}Sr_{0.4})_{0.98}(Co_{0.2}Fe_{0.8})_1O_{3-\delta}$ (LSCF) cathode. Double gadolinium-doped ceria (GDC) catalyst layers with different porosity levels were deposited onto the anode side. The fuels evaluated in this work were carbon black, bituminous coal (Kingwood, WV) and various biomasses, all mixed with a 6% vol Li (53% wt) - K (57% wt) carbonate system. The biomasses were switchgrass, corn stover, and hardwood. Switchgrass was utilized both raw and at different levels of thermal pretreatment (torrefied at 250°C and pyrolyzed at 900°C under inert atmosphere). It was found that torrefied switchgrass presented the highest maximum power density at 800°C ($120.5 \text{ mW}\cdot\text{cm}^{-2}$), as well as the lowest anode polarization resistance ($0.135 \Omega\cdot\text{cm}^2$) when tested in the DCFC. Therefore, corn stover and hardwood were studied just as torrefacted fuels (250°C under inert atmosphere) in the DCFC. Particulate surface area, proximate and ultimate chemical analyses, weight loss upon thermal pretreatment, scanning electron microscopy (SEM), and inductively coupled plasma-optical emission spectroscopy (ICP-OES) of digested biomass samples were carried out on the various fuels to explain differences in performance and anode polarization resistance. A common feature of the three torrefied biomasses is the similar power densities measured at 0.7 V and 800°C, with values of $115 \text{ mW}\cdot\text{cm}^{-2}$ for switchgrass, $112 \text{ mW}\cdot\text{cm}^{-2}$ for hardwood, and $105 \text{ mW}\cdot\text{cm}^{-2}$ for corn stover.

Keywords: Direct Carbon Fuel Cell, biofuel, polarization curves, torrefied biomass, pyrolysis.

1. INTRODUCTION

Biomass is the third largest primary energy source in the world after coal and oil. It remains the primary source of energy for more than half the world's population, providing about 1250 million tons oil equivalent (Mtoe) of energy per year, which is about 14% of the world's annual energy

consumption [1]. Several studies state that bioenergy demand may increase to several hundred exajoules per year in the future; therefore, the development of modernized, sustainable bioenergy systems is necessary for both industrialized and developing countries [2].

Biomass can be transformed into energy (bio-energy) and fuels through a wide range of technologies that can be classified as direct combustion, thermochemical, or biochemical processes [3]. The direct combustion process consists of burning the biomass in air to produce heat, mechanical power, or electricity within a variety of process units, e.g. stoves, furnaces, boilers, steam turbines, and turbo-generators [4]. Among the thermochemical processes, the most referenced in the literature are pyrolysis [5-11], gasification, [11-17], carbonization [18-21], and catalytic liquefaction [22-25]. Anaerobic fermentation [26-28], methane production in landfills [29-31], ethanol fermentation [32, 33], and biodiesel production [34, 35] are the most important biochemical conversion technologies for biomass conversion to energy and fuels.

Apart from the previously mentioned technologies, there are several other processes being developed which involve the utilization of biomass in fuel cells. Gasification of biomass is one route to produce a gaseous fuel, which after cleaning and conditioning, can be sent to a Solid Oxide Fuel Cell (SOFC) [36-41]. However, various researchers have indicated that higher efficiencies and lower logistical costs may be realized within a so-called Direct Carbon Fuel Cell (DCFC) by utilizing the solid biomass directly as a fuel without reforming or cleaning. The DCFC can cleanly convert the chemical energy of solid carbon directly into electricity through the electrochemical oxidation of C in the anode chamber to CO₂ with the release of four electrons. The oxidation involves several reaction steps, including the Boudouard reaction, partial oxidation of carbon, reactions with the carbonates used for electrical conductivity, etc [42]. These four electrons then reduce oxygen to oxygen ions (O²⁻) at the cathode. The oxygen ions migrate across the electrolyte driven by a chemical potential difference between the electrodes. At the anode, the oxygen ions in turn oxidize the available C fuel. The Direct Carbon Fuel Cell has a potential economic benefit as there is no need for a gasifier, fuel processor, and contaminant filters for its operation. This is especially important on a smaller scale such as 10-10,000 W units for distributed power systems [43]. The overall process of producing electricity in a DCFC from biomass involves only two steps: drying (and/or pyrolysis, hydrothermal carbonization, or torrefaction) to obtain char, and feeding the resulting fuel directly into the DCFC. Drying and/or pyrolysis, torrefaction, or char conversion via hydrothermal carbonization may be required because of the considerable amount of volatile matter within the biomass. Furthermore, the volatile matter and the inorganic constituents within the raw biomass may interfere with the electrochemical reactions of the system and cause performance degradation. [44]. Studies of these effects have not been completed to date.

There are studies which discuss the use of coal as fuel in DCFCs [45-51]. These works identified several issues hindering performance due to mass transfer limitations at high current densities (leading to concentration polarization in the system) and the large activation loss in the anode side because of the sluggish kinetics of the electrochemical oxidation of solid carbon. These works primarily focus on the effect of the coal source and fuel cell design on the performance. Over the past few years, more attention has been focused upon the use of biomass as fuel in the Direct Carbon Fuel Cell. Adeniyi [52] has investigated the use of six different pyrolyzed biomasses (miscanthus,

switchgrass, wheat, spruce, poplar and willow) in the DCFC. This group investigated two electrolyte systems: molten carbonate electrolyte direct carbon fuel cell (MCDCFC) and solid oxide electrolyte direct carbon fuel cell (SODCFC). Miscanthus showed the highest open circuit voltage for the SODCFC (1.24V), reporting a maximum power density of $\sim 77 \text{ mW}\cdot\text{cm}^{-2}$, while willow showed an open circuit voltage of 0.83 V and a maximum power density of $\sim 18 \text{ mW}\cdot\text{cm}^{-2}$ for the MCDCFC. Ahn *et al.* [44] utilized wood biomass char in a stirred Li-K carbonate MCFC system and reported a maximum power density of $\sim 41 \text{ mW}\cdot\text{cm}^{-2}$ at 873°K. Recently, Dudek *et al.* [53] focused on utilizing raw beech and acacia wood waste as fuel in a SODCFC, which showed promising maximum power densities of $\sim 100 \text{ mW}\cdot\text{cm}^{-2}$ at 800°C. This work was interesting since the wood was not excessively pre-treated. Elleuch *et al.* [54 55] and Yu *et al.* [56] have both recently reported operating a different MCDCFC architecture with biochar fuels. The fuel cell architecture was based on a $\text{Li}_2\text{CO}_3/\text{Na}_2\text{CO}_3/\text{Ce}_{0.8}\text{Sm}_{0.2}\text{O}_{1.9}$ electrolyte with a LiNiO_2 cathode. The olive wood [54] and almond shell [55] biochar fuels were pretreated at 600°C in N_2 , while the corn cob biochar was processed at 700°C in N_2 . The works by Elleuch *et al.* and Yu *et al.* displayed maximum power densities between $\sim 100\text{-}127 \text{ mW}\cdot\text{cm}^{-2}$ at 700°C on these biochars, which are some of the highest performances reported for DCFCs using biomass derived fuels.

Many of the works described above investigated the effect of char chemistry and carbon structure on the electrochemical performance, where the biomass source was typically fully pyrolyzed. To the best of our knowledge, there are no studies that compare the effect of thermal treatment of the biomass fuel on the electrochemical performance. The present paper investigates the effect of torrefaction and pyrolysis thermal pretreatments on hardwood, corn stover, and switchgrass biomass. The resultant processed biomass was incorporated as the fuel within the DCFC and electrochemically tested between 650-800°C. As a baseline, the performance of the DCFC with carbon black and bituminous coal is also reported. The detailed features of the DCFC in the present work, in terms of anode structure and anodic mixture composition, were presented elsewhere [57].

2. EXPERIMENTAL

2.1. Electrolyte preparation

The evaluation of coal and biomass with different pretreatments as a fuel source in the DCFC was the prime interest of this work. The electrolyte-supported fuel cell architecture previously developed was selected as the platform for these studies [57]. The electrolyte-supported button cells were fabricated using a conventional tape-casting technique [58]. A high-purity commercial electrolyte material, 8YSZ powder (Daiichi Kigenso Kagaku Kogyo Co., LTD, Japan), was dried and conditioned by ball-milling for ~ 24 h with an organic dispersant, plasticizer and binder to form a tape-casting slurry. The slurry was then cast by laboratory-scale tape-casting equipment. The blade gap was set to 100 μm . Three tapes of the electrolyte were stacked together and laminated under a pressure of 75 klb_f for 15 min via a laboratory press at 100°C. After final shaping by a laser cutter, a two-stage sintering procedure and a forging process were applied. In the first step, the organic materials were

burned out with a slow heating schedule up to 1000°C. After this stage, the half-sintered substrates were transferred to a high-temperature furnace where they were heated to 1450°C to achieve a relative density of 98% (measured by the Archimedes method) [59]. To assure total flatness of the substrates, a forging process (where the substrates are heated at 1400°C for 6 h between two flat plates) was performed. The substrates had a final dimension of 4 cm diameter, an average thickness of ~140 μm and an average density of 99% theoretical.

2.2. Single-cell preparation

GDC powders were synthesized by solid-state reactions using cerium ammonia nitrate (Alfa Aesar) and gadolinium carbonate hydrate (Alfa Aesar) as precursors [60]. These powders were mixed with Johnson Matthey ink vehicle and diluted fish oil at a suitable ratio to prepare the screen-printing paste. The paste was deposited at the center of both sides of the YSZ substrate (active area of ~2.85 cm²) using a DEK Model 248 screen-printer. The final samples were sintered at 1300°C producing a GDC layer of 3-7 μm thick. An extra layer of GDC was printed over the initial thin layer on the anode side, which contained rice starch as a pore former (50-50 vol%). This second porous GDC layer displayed an average thickness of 50 μm and a porosity of 35% measured by SEM imaging with ImageJ software. As stated in previous work [57], the GDC layers on the anode side act as catalyst layers for enhancing the electrochemical oxidation of carbon, with the porosity of the porous GDC layer facilitating the electron conductivity and increasing the area of the triple-phase boundary. GDC was introduced as a diffusion barrier layer on the cathode side due to its high ionic conductivity and low reactivity with Sr-containing cathodes [61].

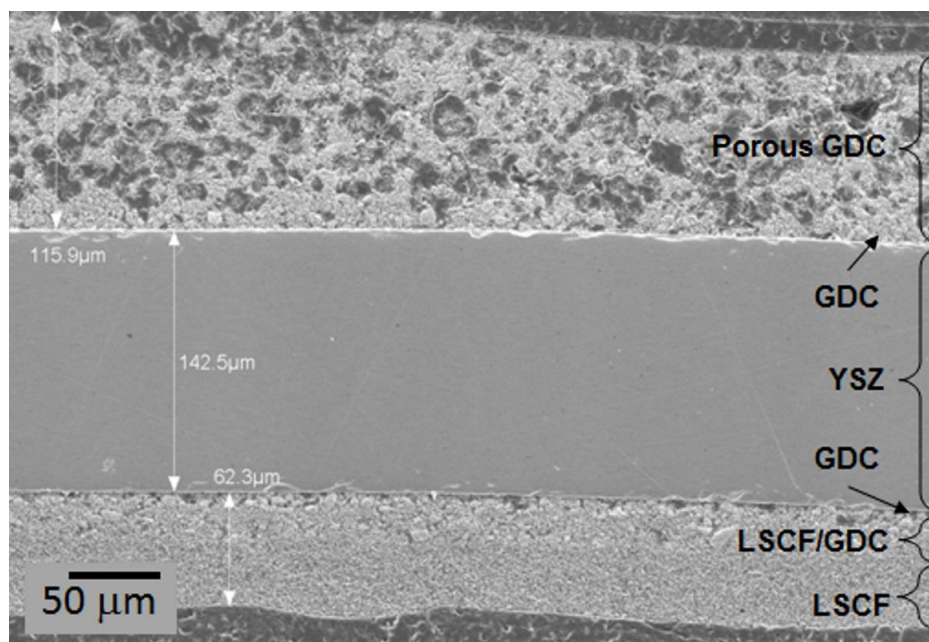


Figure 1. Cross-sectional SEM micrograph of a non-tested direct carbon fuel cell with a YSZ solid electrolyte at 400X magnification.

The LSCF cathode powders were synthesized by attrition milling and calcination at 1100°C for 2 h in air using the raw material sources of La_2O_3 , SrCO_3 , CoCO_3 , and Fe_2O_3 . The final LSCF powder was mixed with GDC powder to prepare the screen printing paste for the active cathode layer which was screen-printed over the GDC barrier layer on the cathode side of the substrate. This active layer was dried prior to screen-printing a pure LSCF current collector layer over the previous layer. The average thickness of the active layer was 5-8 μm , while for the current collector layer the thickness was ~17-21 μm . The active and the current collector layers were sintered together at 1000°C for 2 h in air. Figure 1 displays the scanning electron micrograph of the final cell cross-section (SEM, Hitachi S-4700).

All the anodic fuel compositions in the present study included Li_2CO_3 (Fisher Chemicals) - K_2CO_3 (Acros) (68 mol % Li_2CO_3 (53 wt%)- 32 mol % K_2CO_3 (47 wt %)) mixed by ball-milling with the carbon black (Fisher Chemicals), Kingwood (West Virginia) bituminous coal and different biomass fuel sources at a ratio of 6 vol% carbonates/fuel. This anodic composition of inorganic/organic material was previously verified as showing the highest performance for this specific cell configuration [57]. A cell using carbon black as the fuel source was tested for base-line performance.

2.3. Electrochemical testing

For testing purposes, each single cell was sealed between a 4 cm OD and 2 cm ID alumina tube and an alumina washer with the same dimensions using a mica ring and Aremco Ceramabond® cement, with the anode side bonded within the tube. The cell was filled with the powdered anodic mixture until it occupied approximately two-thirds of the volume of the alumina tube. The sealed fuel cell was placed into the fuel-cell test stand and heated to 650°C while flowing preheated argon (30 sccm) and air (50 sccm) to the anode and cathode chambers, respectively. The electrochemical testing for the biomass fuels was performed at 650, 800, and 750°C (in this specific order) while for carbon black and coal the order was 650, 700, 750, and 800°C. The temperature of the cell was measured on the anode side by a type-K thermocouple placed a few millimeters above the carbon/carbonate mixture. A cross-section of the testing set up can be found in a previous paper [57]. Silver mesh and wire were attached to the cathode and anode surface with LSCF ink and Pt ink, respectively, for current collection. The cells were electrochemically characterized using a galvanostat/potentiostat (Solartron 1287A, Solartron Analytical, England). The voltage-current-power (V-I-P) plots were constructed by applying a current load to the cell that increased in a stepwise fashion at 2 mA/s, and proceeded until the cell voltage reached 0 V. After electrochemical testing, the cell was cooled in argon to room temperature for further observation.

2.4. Characterization of fuels

The biomasses in the present study, along with their corresponding pretreatment and weight loss (mass difference before and after thermal processing), are summarized in Table 1. For the pyrolytic thermal treatment, the biomass was heated at a rate of 1°C/min until 900°C and held there

isothermally for 1 h under an inert N₂ atmosphere. Torrefaction was performed at 250°C under N₂ with the same heat-up rate. SEM was used to characterize the microstructure of the different biomasses and the ASAP 2020 (Micromeritics Co., USA), applying the Brunauer–Emmett–Teller (BET) equation, was used to determine the surface area with nitrogen gas at 77.15 K. The adsorption and desorption tests were performed at relative pressures $P/P_0 = 0.05–0.95$ and $P/P_0 = 0.95–1.0$, respectively. The specific surface areas (S_{BET}) of the samples were acquired at relative pressures $P/P_0 = 0.05–0.2$ (Table 2). The proximate analysis for the biomasses, shown in Table 3, was performed according to ASTM D3172-07 with a LECO 701 Thermo-Gravimetric analyzer. The elemental analysis of the same samples (used for the quantitative determination of carbon, nitrogen, hydrogen, and sulfur, with high accuracy and sensitivity) as shown in Table 4, was performed using a ThermoQuest Elemental Analyzer, FLASH EA112 series, according to ASTM D3176. The biomass was added to the carbonate mixture in the appropriate ratio and the mixture was ball-milled in isopropanol for 24 h, dried, and sieved using a number 60 (250 μm) sieve.

Table 1. Biomasses tested in this study along with their pretreatments and weight loss expressed as the weight difference before and after the thermal pretreatment.

Biomass	Pretreatment	Weight loss upon heating (wt%)
Switchgrass	Raw	N/A
	Torrefied	25
	Pyrolyzed	73
Hardwood	Torrefied	30
Corn stover	Torrefied	28

Table 2. Surface area (BET ASAP 2020) of the different fuels tested in the present study. The confidence interval is shown for each measurement.

Carbon source	Surface area (m ² ·g ⁻¹)	Confidence interval (m ² ·g ⁻¹)
Carbon black	30.327	0.0598
Bituminous coal	1.009	0.0088
Torrefied switchgrass	0.736	0.0053
Pyrolyzed switchgrass	30.519	0.8641
Torrefied hardwood	0.532	0.0244
Torrefied corn stover	0.652	0.0095

Table 3. Proximate analysis of the different fuels tested in the present study.

Sample	Moisture (%wt)	Volatile (%wt)	Ash (%wt)	Fixed Carbon (%wt)
Carbon black	0.45	3.14	0.00	96.41

Bituminous coal	0.95	31.87	9.49	57.69
Raw switchgrass	6.70	74.56	2.84	15.90
Torrefied switchgrass	1.19	68.16	3.86	26.75
Pyrolyzed switchgrass	1.30	3.38	10.44	84.85
Torrefied hardwood	2.60	74.26	0.30	22.89
Torrefied corn stover	3.39	35.43	20.16	41.02

Table 4. Elemental analysis of the carbon black, coal, and the different biomass.

Component Name / (%wt)	Nitrogen	Carbon	Hydrogen	Sulfur	Oxygen
Carbon black	3.27	97.36	0.00	0.56	0.00
Bituminous coal	3.61	77.84	5.12	1.01	12.42
Raw switchgrass	1.89	45.38	6.21	0.00	46.52
Torrefied switchgrass	2.63	50.59	5.77	0.00	41.01
Pyrolyzed switchgrass	2.71	85.32	0.00	0.00	11.97
Torrefied hardwood	2.16	51.86	6.22	0.00	39.76
Torrefied corn stover	2.40	54.17	4.25	0.04	39.14

3. RESULTS AND DISCUSSION

3.1. Baseline experiments: non-biomass fuels

In order to provide a baseline for the subsequent biomass experiments, carbon black was tested as fuel in the DCFC.

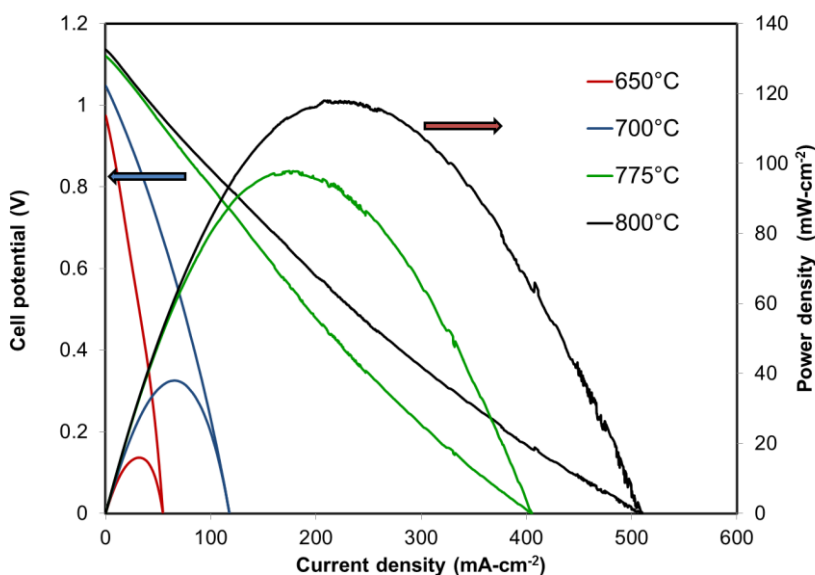


Figure 2. V-I-P curves for the cell tested with carbon black as fuel at 650, 700, 775, and 800°C.

Carbon black was selected for these preliminary experiments because of its homogeneity (pure carbon as opposed to coal and biomass), and electrical conductivity [62]. The results of these tests over the temperature range of 650-800°C are shown in Figure 2 where the voltage vs. current density, and power density vs. current density are combined in the same chart (V vs. I represented using the left y axis, P vs. I represented using the right y axis). The Open Circuit Voltage (OCV) ranged from 0.9 to 1.65V at 650 and 800°C respectively, with the maximum power density reaching 118 mW·cm⁻² at 800°C. This result represents an improvement with respect to our previous work [57], where the maximum power density at 800°C was found to be 71 mW·cm⁻². This difference can be explained by observing the ohmic resistance of both systems at 800°C, showing that the ohmic resistance of the cell presented in Figure 2 was 1.4 Ω·cm², while the ohmic resistance of the cell tested in our previous work [57] was 2.6 Ω·cm², indicating a correlation between ohmic resistance and cell performance consistent with Ohm's law. According to the literature, the electrolyte can sometimes account for 80% of the ohmic resistance of the cell [63].

Raw as-received bituminous coal (Kingwood, West Virginia) was substituted for the carbon black as the fuel in the anode compartment. According to the BET analysis in Table 2, the coal presents much less surface area than carbon black, which affects the amount and availability of active sites for the carbon oxidation in the anode chamber. This lower surface area should in turn translate to a decrease in performance compared with Figure 2 for the carbon black. As shown in Figure 3, the performance of the DCFC with the coal fuel is lower than that of the carbon black.

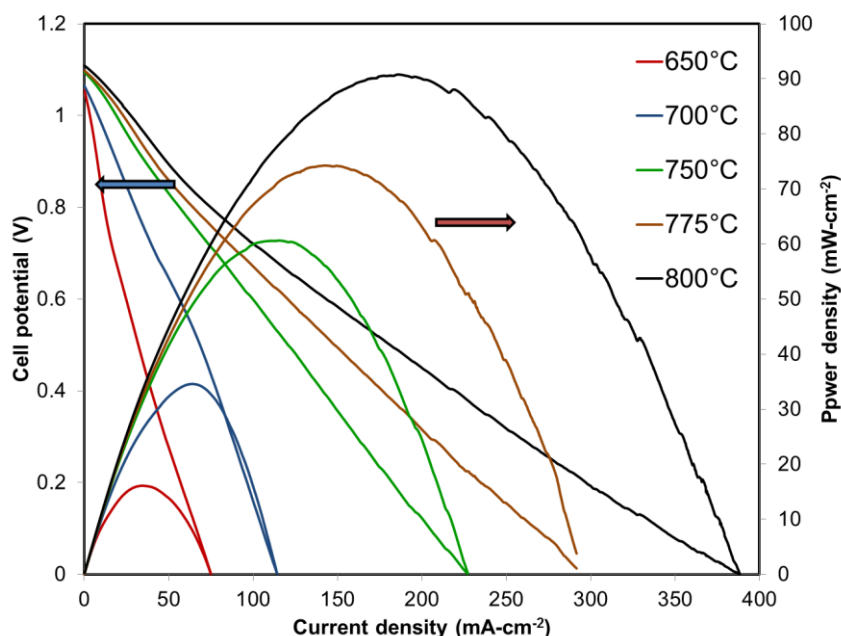


Figure 3. V-I-P curves for the cell tested with Kingwood bituminous coal as fuel at 650, 700, 750, 775, and 800°C.

Relating the results of the electrochemical tests for carbon black and bituminous coal (Figures 2 and 3) with the values of surface area for both fuels (Table 2), it is obvious that the surface area of the fuel is not a critical factor dictating the performance of the DCFC. Carbon black possesses 30

times more surface area than Kingwood bituminous coal, but it performs (considering maximum power density at 800°C) only 20% better than bituminous coal. Considering the elemental analysis of both samples shown in Table 4, carbon black contains a higher amount of carbon than the bituminous coal and hence more carbon is available for oxidation. Further analysis of this observation with biomass as fuel below will confirm this trend.

3.2. Biomass experiments

Biomass was next tested as fuel in the DCFC system. As reported by El-Nashaar *et al.* [64], native grasses harvested along roadways or buffer strips to control weed proliferation in the Pacific Northwest of the US, may provide feedstock to supply 8% of the current electrical and transportation energy consumption for that region. However, the mineral content of grasses could limit their direct utilization for bioenergy production in a fuel cell system. At high operational temperatures, sodium and potassium (and other alkalis and alkaline-earths) present in crop residues (such as corn stover) can vaporize, react with other mineral components (silica) and form a sticky glass-like substance known as slag [64, 65]. The slag could then corrode the structures of the fuel cell system reducing its operational life time. The amount and type of minerals in any biomass feedstock depend on the soil, the developmental stage at harvesting, time of harvesting, the species, and the part of the plant selected as the feedstock [64].

3.3. Switchgrass pretreatment comparison

Switchgrass (*Panicum virgatum* L.) is a warm-season perennial grass that is native to the prairies of North America and grown in monoculture for hay, grazing, and erosion control. It has received considerable interest because its cultivation can produce high yields of good quality biomass during hot, dry midsummer days when cool season grasses such as tall fescue (*Festuca arundinacea* Schreb.) are unproductive. Its wide adaptation is also a very important factor [66, 67].

In this work, raw and thermally pretreated switchgrass were tested in the DCFC. The pretreatment is important since it removes the moisture and volatile matter within the biomass that could disrupt the electrochemical reactions in the system [44]. However, the pretreatment process involves an energy input whose economics must be evaluated in terms of the overall energy balance of the process. Two thermal processes were employed in this work to pretreat the switchgrass: 1) pyrolysis at 900°C and 2) torrefaction at 250°C (both performed in an inert atmosphere of nitrogen for 1 h at temperature). This pretreatment affects the microstructure (Figure 4), the surface area, (Table 2), and the proximate and elemental composition of the switchgrass (Table 3 and 4, respectively).

SEM micrographs of the raw and pretreated switchgrass are presented in Figure 4. Comparing the images of the pyrolyzed (Figure 4 a) and torrefied (Figure 4 b) switchgrass, an increase of porosity is observed in the biomass structure as the temperature of the thermal pretreatment increases. This explains the significant increase of BET surface area between the pyrolyzed and torrefied switchgrass (Table 2). The thermal pretreatment of the switchgrass also impacts the proximate analysis as shown in

Table 3, where the ash and fixed carbon contents of the switchgrass increase, and the volatile matter decreases as the temperature of the pretreatment increases. With respect to the elemental composition, the percentage of carbon dramatically increases, while the percentage of hydrogen decreases as the temperature of the pretreatment increases. These results were expected because the pretreatment has the objective of removing light hydrocarbons and volatile species from the biomass.

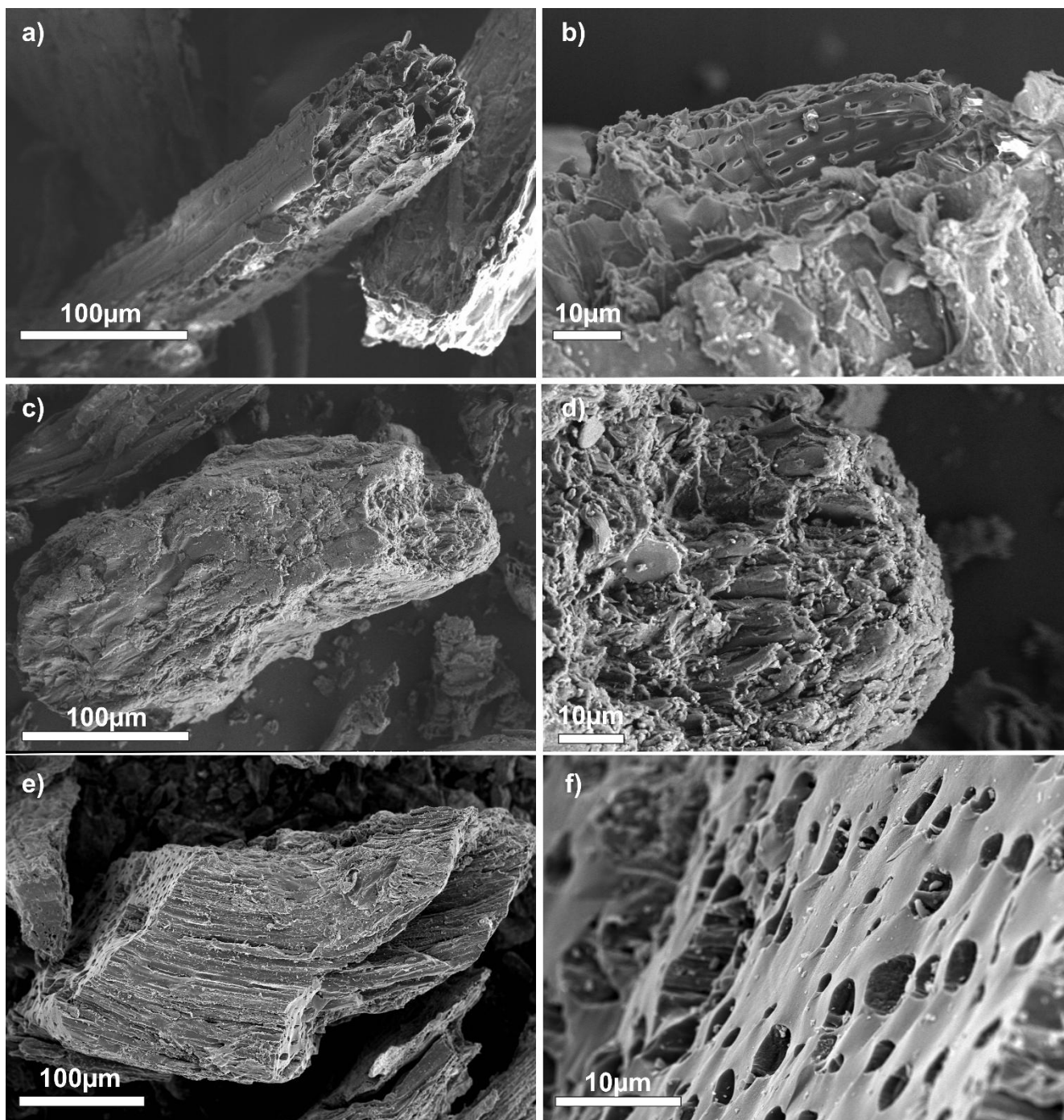


Figure 4. SEM images of the raw (a,b), torrefied (c,d), and pyrolyzed switchgrass (e,f) used as fuels in the Direct Carbon Fuel Cells. Raw and torrefied switchgrass micrographs present a magnification of 400X (a,c) and 1500X (b,d), while pyrolyzed switchgrass micrographs present magnifications of 300X (e), and 3000X (f).

The raw and pretreated switchgrass samples (along with the Li-K carbonate binary system) were loaded in the anode chamber of a DCFC system, and tested starting at 650°C and continued to 800°C. A compilation of the results of the electrochemical tests, in terms of maximum power density ($\text{mW}\cdot\text{cm}^{-2}$) is presented in Figure 5.

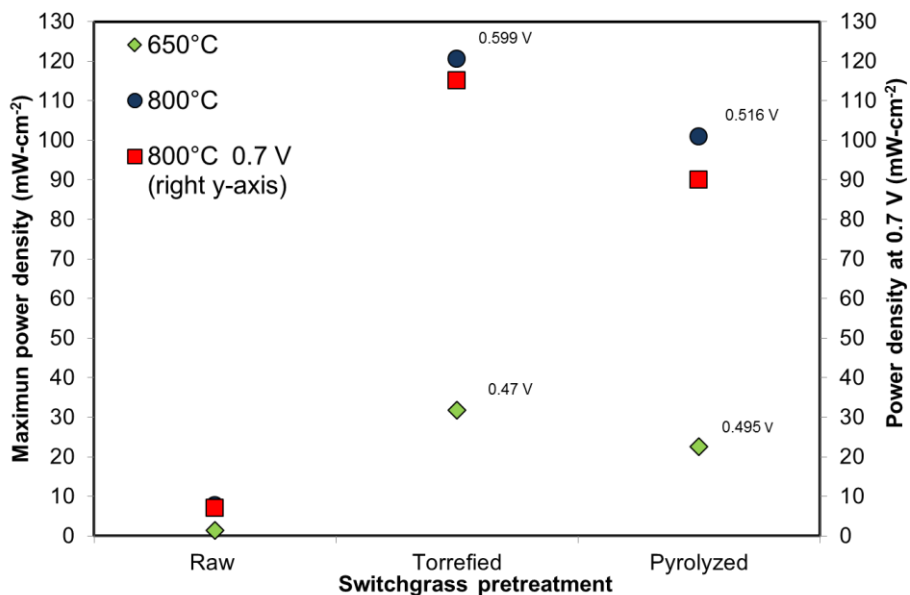


Figure 5. Maximum performance and performance at 0.7 V for the cells tested at 650 and 800°C using raw switchgrass and switchgrass with different thermal pretreatments (torrefaction and pyrolysis). Also shown in the graph are the voltages where those maximum performances are achieved.

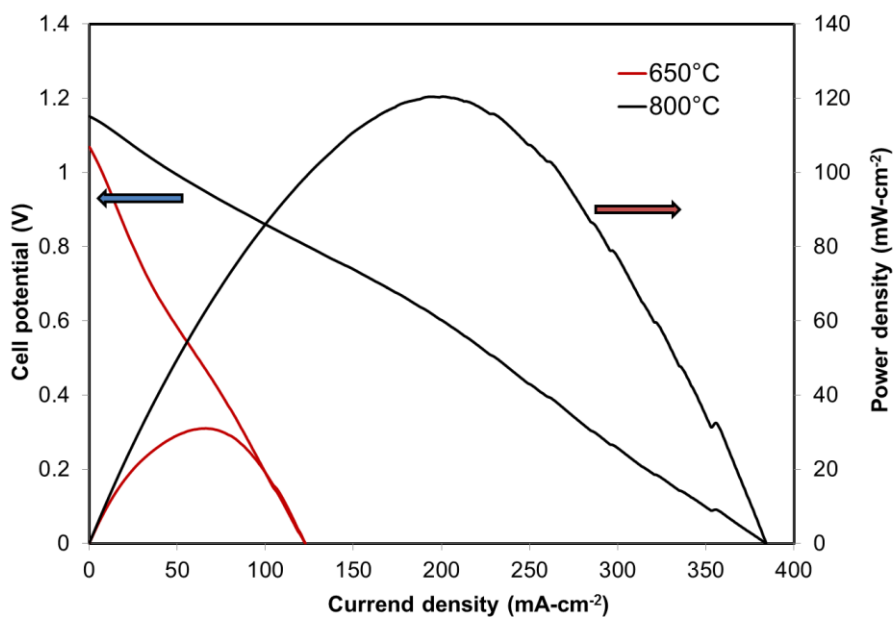


Figure 6. V-I-P curves for the cell tested with torrefied switchgrass as fuel at 650 and 800°C.

It is observed that higher testing temperature leads to higher performance of the cell, partially because of the increase of the ionic diffusion of oxygen ions through the YSZ electrolyte which decreases the ohmic resistance of the cell [57]. Figure 5, showing the maximum power density and power density at constant cell voltage of 0.7 V at 650 and 800°C, demonstrates that a pretreatment of biomass is necessary to reach acceptable performance. However, the extent of switchgrass thermal pretreatment has a limited positive effect in the performance of the cell, i.e., the extra energy input for the biomass pretreatment beyond torrefaction is not justified by a significant increase in cell performance. Figure 6 shows the V-I-P performance curves for torrefied switchgrass at 650 and 800°C. The OCV of the cells also differs depending of the pretreatment at the same temperature, suggesting different reaction paths for the electrochemical oxidation of carbon. At 650°C, the OCV for the cell tested using raw biomass as fuel is 1.03 V, while for the torrefied switchgrass it is 1.08 V, and 1.01 V for the pyrolyzed sample. It also changes with temperature, since for 800°C the OCV for the raw switchgrass is 1.1 V, while for the torrefied and pyrolyzed samples, it is 1.15, and 1.13 V, respectively. The mechanism of electrochemical oxidation of carbon is complicated and the existing literature on this topic is scarce [45] and is beyond the objective of this paper.

3.4. Torrefied biomass

In this section, the electrochemical performance is compared for the DCFC operating with torrefied switchgrass, corn stover and hardwood as fuels. Torrefaction was chosen as the biomass pretreatment protocol based on the performance results for switchgrass, and the assumption that the same trend would apply to hardwood and corn stover. Figures 7 and 8 show the polarization curves (V-I-P) for torrefied hardwood and torrefied corn stover, respectively.

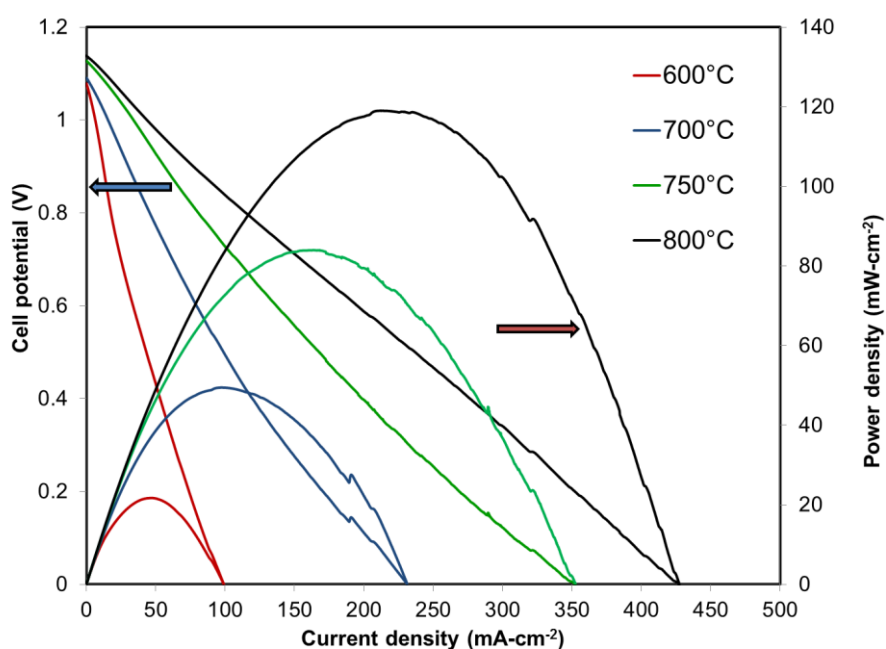


Figure 7. V-I-P curves for the cell tested with torrefied hardwood as fuel at 650, 700, 750, and 800°C.

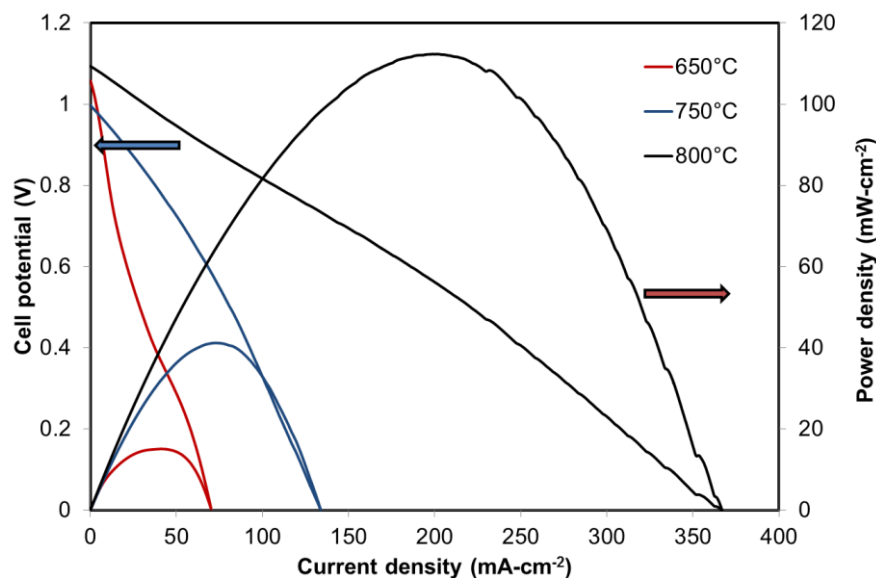


Figure 8. V-I-P curves for the cell tested with torrefied corn stover as fuel at 650, 750, and 800°C.

It is observed that for every temperature tested, torrefied hardwood performs better than torrefied corn stover in the DCFC. Figure 9 presents SEM images of both torrefied biomasses to establish differences in microstructure that could explain the variation in performance observed in Figures 7 and 8. According to SEM, torrefied corn stover particles are five times smaller than torrefied hardwood particles (comparing biggest corn stover particles with smallest torrefied hardwood particles) and the hardwood appears to show more surface structure. These two differences (particle size and surfaces area) were originally thought to have a strong influence on the electrochemical oxidation of carbon in the anode chamber, and therefore, on the cell performance. However, the results are quite similar suggesting that particle size and surface area are not critically important factors to consider in determining cell performance.

Table 5 shows the values of the current and power densities at 0.7 V measured at 800°C for the various fuels presented here. This cell voltage is a common point of comparison when assessing the relative operation of fuel cells, and differs from the maximum values of power and current density as shown in Figure 5. As observed in Table 5, coal exhibits lower performance than carbon black when fueling the DCFC. This can be explained by a combination of factors that contribute adversely to the cell performance when using Kingwood bituminous coal. The first is that coal has about 20% less carbon than the carbon black (77% carbon for coal vs. 97% carbon for carbon black). Thus less carbon is available for reaction. The second is the higher concentration of sulfur and inorganic matter in the coal, both of which can act as poisons in the anode compartment [62]. The presence of sulfur in torrefied cornstover can also explain the lower performance for this fuel (Table 4), considering these two fuels are very similar in terms of surface area and fixed carbon content. With respect to the different thermal pretreatments of the switchgrass, torrefaction delivers the highest performance,

nearly 20% higher than that of the pyrolyzed switchgrass. In fact, all the torrefied samples showed better performance than the pyrolyzed switchgrass.

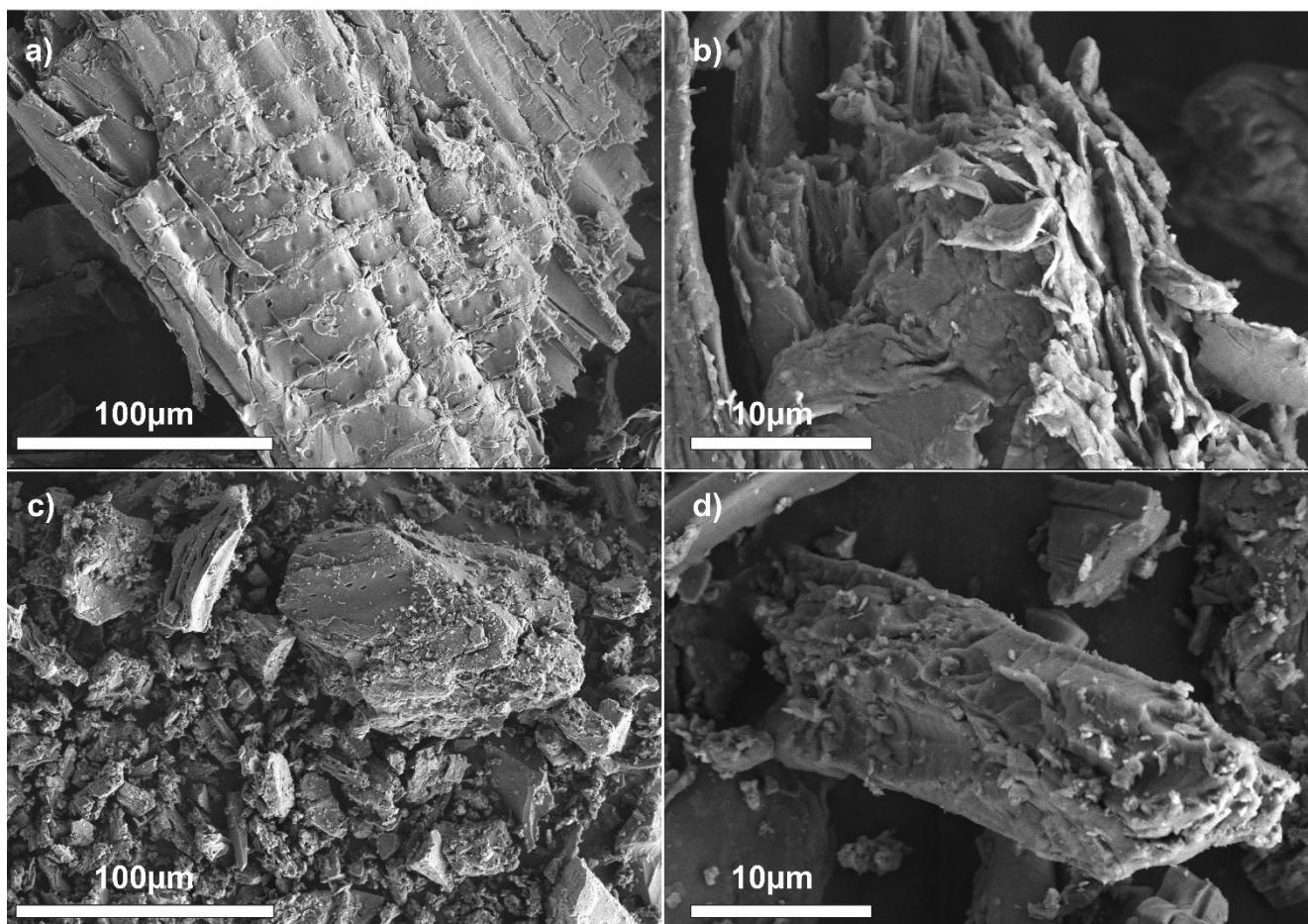


Figure 9. SEM images of torrefied hardwood (a,b), and torrefied corn stover (c,d) used as fuels in the Direct Carbon Fuel Cell. Torrefied hardwood and corn stover micrographs present a magnification of 500X (a,c) and 3500X (b,d).

Table 5. Values of current density and power density for the different fuels tested at a voltage of 0.7V and a temperature at 800°C.

Values at 0.7V and 800°C	Current density (mA·cm ⁻²)	Power density (mW·cm ⁻²)
Carbon black	160	112
Coal	120	84
Raw switchgrass	10	7
Torrefied switchgrass	165	115
Pyrolyzed switchgrass	130	90
Torrefied hardwood	160	112
Torrefied corn stover	150	105

Finally, it is interesting to observe how the inorganic constituents present in the biomass could affect the performance of the cell. The trace elements chosen for analysis were B, Al, Ba, Ca, Mg, Mn, Ni, K, Na, Zn, and P, as suggested by the existing literature in the area [64, 68]. Cobalt and molybdenum were also analyzed, but the results for these elements were lower than the detection limit of the analytical method. The minerals were extracted from the raw biomass using microwave-assisted acid digestion (Environmental Protection Agency (EPA) method 3052) and analyzed by ICP-OES. Table 6 shows the concentration of each element in ppm (mg L^{-1}). It is assumed that these trace elements are retained in the biomass sample after thermal treatment, but in a more concentrated form.

Table 6. Microelemental analysis for hardwood, switchgrass and corn stover using ICP-OES with predigested biomass using nitric acid as stated in EPA method 3052. The method detection limit is provided for every element analyzed. All results are in ppm.

Analyte	B	Al	Ba	Ca	Mg	Mn	Ni	K	Na	Zn	P
Method Detection Limit (ppm)	0.009	0.1	0.012	0.1	0.1	0.1	0.01	0.1	0.1	0.013	0.047
Hardwood	0.074	0.36	0.169	10.37	1.73	2.46	<0.01	4.81	0.274	0.116	<0.047
Switchgrass	0.071	11.43	0.233	24.58	6.56	1.5	0.033	9.33	0.64	0.307	5.831
Corn stover	0.065	13.51	0.208	34.52	10.55	0.396	0.012	108.01	0.27	0.213	6.607

Using the elemental analysis in Table 6 with the performance data in Figures 6, 7, and 8 (summarized in Table 5), it is observed that the change in the trace element composition does not translate to significant differences in performance of the cells fueled with those biomasses (using the given Li-K carbonate composition at the specific fuel/carbonate ratio). Torrefied switchgrass shows the best performance among the fuels studied here, however the concentrations of all its trace elements are between those for hardwood and corn stover. Thus, it can be concluded that none of the analyzed trace elements act either as a catalyst or a poison for the electrochemical process at least in these concentrations (for the given anode composition). Special interest is to be placed on the difference in potassium among the three biomasses since potassium is known to have a strong catalytic effect in carbon oxidation [42]. According to the ICP analysis, the amount of potassium in corn stover is more than ten times higher than in switchgrass and more than 25 times higher than that in hardwood. This difference does not translate to a positive change in performance for corn stover. However, any effect of the naturally-occurring potassium in the biomass would be overwhelmed by the extremely large amount of potassium carbonate in the anodic chamber (around 10 wt% potassium carbonate), making the amount of naturally contained potassium in the biomass negligible.

3.5. Electrochemical Resistance Analysis

The values of ohmic and polarization resistances for the cells operating with the different fuels are evaluated by means of the V/I curves obtained for each test at 800°C. The results are shown in

Table 7. The total resistance of the cell ($\text{ohms}\cdot\text{cm}^2$) was calculated from the slope of the polarization curves (V vs. I) near the Open Circuit Voltage (i.e., the slope on the V/I curve near a current density of 0). Specifically, it was taken considering the V/I data until a load of 6mA was drawn in the cell in all cases (3 seconds after the test started). The ohmic resistance of the cell is taken from the flat region of the V/I curve (with three data points when a current of 150 mA was drawn in the cell). The polarization resistance of the cell is calculated by subtracting the value of the ohmic resistance from the total resistance of the cell. This polarization resistance gives information about the intrinsic operation of both electrodes (anode and cathode). Considering that the cathode in all of the cells has the same composition and tri-layer structure, the value of the cathode polarization resistance was assumed to be identical for all the cells. It was measured as $0.085 \text{ ohms}\cdot\text{cm}^2$ at 800°C by using a symmetric electrolyte-supported fuel cell (i.e., the same cathode printed on both sides of the electrolyte). By subtracting the cathode polarization resistance from the polarization resistance of the entire cell, the value of polarization resistance of the anode alone can be estimated [57].

Table 7. Values of the total resistance (slope of the polarization curves near OCV), ohmic resistance, and polarization resistance for the DCFCs tested using different fuels and pretreatments at 800°C .

Fuel	Total resistance ($\text{Ohms}\cdot\text{cm}^2$)	Ohmic resistance ($\text{Ohms}\cdot\text{cm}^2$)	Polarization resistance ($\text{Ohms}\cdot\text{cm}^2$)	Anode polarization resistance ($\text{Ohms}\cdot\text{cm}^2$)
Carbon black	2.55	2.27	0.28	0.195
Bituminous coal	3.15	2.84	0.31	0.225
Raw switchgrass	N/A	N/A	N/A	N/A
Torrefied switchgrass	2.59	2.37	0.22	0.135
Pyrolyzed switchgrass	3.68	2.87	0.81	0.725
Torrefied hardwood	2.69	2.39	0.30	0.215
Torrefied corn stover	2.86	2.57	0.29	0.205

Comparing the results in Tables 5 and 7, it is clear that a decrease in anode polarization resistance of the cell leads to higher performance at a voltage of 0.7 V at 800°C . Also by comparing the results in Table 7 with the values of the BET surface area in Table 2, it can be stated that the performance of the cell does not correlate with the surface area of the fuel. For example, the values of the BET surface area for carbon black and pyrolyzed switchgrass are very similar. However, the anode polarization resistance is much higher for pyrolyzed switchgrass than for carbon black. Further, when comparing surface areas of the torrefied and pyrolyzed switchgrass, the increase of surface area of the pyrolyzed sample led to lower performance as compared to the one using the lower-surface area torrefied switchgrass. Thus, at least for the samples tested here, there does not appear to be a direct correlation between the performance of the fuel in the DCFC and the surface area, elemental composition and the amount of trace inorganic elements.

4. CONCLUSIONS

An electrolyte-supported direct carbon fuel cell, with a multi-layered LSCF cathode and a dense/porous GDC anode layer, was used for testing different biomasses with various pretreatments. Initial experiments were focused on establishing a testing baseline using carbon black and coal as the carbon source. The performance of raw and pretreated switchgrass with different thermal processes (torrefaction and pyrolysis) was assessed. The low performance obtained in the cells tested with raw switchgrass indicated the efficacy of a thermal pretreatment of the biomass. However, it was demonstrated that the increase of the pretreatment temperature beyond that for torrefaction does not have a positive effect on the utilization of the switchgrass in the fuel cell. Indeed, the performance of the cell at a voltage of 0.7 V and 800°C decreased by 20% when utilizing pyrolyzed switchgrass as the fuel. Considering torrefaction as the most suitable pretreatment process for switchgrass (not only in terms of performance in the fuel cell, but also in terms of the overall energy balance of the process), this pretreatment was also applied to hardwood and corn stover. The performance of those fuels was similar, but slightly lower than that obtained using torrefied switchgrass. These results have been confirmed by evaluating both the V-I-P measurements and the anodic polarization resistance at 800°C.

In order to investigate the differences in performance, the biomasses have been fully characterized in terms of surface area (BET), microscopy (SEM), proximate and ultimate analysis, and trace elemental analysis through acid digestion and ICP-OES. Relating the performance of the cells with the characteristics of the biomass, it was demonstrated that neither the surface area nor the amount of fixed carbon in the fuel exhibited a positive influence in the performance of the cell. Sulfur was in low concentration (if any) in the samples. The presence of the trace elements in the samples does not appear to show any catalytic or poisoning activity. The influence of potassium (well-known as an active catalyst for the oxidation of carbon) contained in the biomass showed low influence on performance, since the high potassium level in the carbonate anode mixture masked any effect.

ACKNOWLEDGMENTS

The authors would like to thank Fundacion Caja Madrid (Spain), WVU Advanced Energy Initiative (AEI) program, US DOE Office of Basic Energy Sciences, NETL (National Energy Technology Laboratory), WV State EPSCoR Office, and West Virginia University under grant number DE-FG02-06ER46299. The authors would also like to acknowledge Anna McClung, Jeremy Hardinger and Areej Kuzmar for assistance with characterization and electrochemical testing.

References

1. L. Chen, L. Xing, L. Han, *Renewable and Sustainable Energy Reviews*, 13 (2009) 2689.
2. G. Berndes, M. Hoogwijk, R. Broek, *Biomass and Bioenergy*, 25 (2003) 1.
3. <http://www.fao.org/docrep/T1804E/t1804e06.htm>. Last accessed 06/25/2013.
4. P. McKendry, *Bioresource Technology*, 82 (2002) 47.
5. J.E. White, W.J. Catallo, B.L. Legendre, *Journal of Analytical and Applied Pyrolysis*, 91 (2011) 1.
6. Q. Lu, C. Dong, X. Zhang, H. Tian, Y. Yang, X. Zhu, *Journal of Analytical and Applied Pyrolysis*, 90 (2011) 204.

7. N. Jendoubi, F. Broust, J.M. Commandre, G. Mauviel, M. Sardin, J. Lede, *Journal of Analytical and Applied Pyrolysis*, 92 (2011) 59.
8. G. Varhegyi, M.J. Antal, E. Jakab, P. Szabo, *Journal of Analytical and Applied Pyrolysis*, 42 (1997) 73.
9. J. Yanik, R. Stahl, N. Troeger, A. Sinag, *Journal of Analytical and Applied Pyrolysis*, 103 (2013) 134.
10. F.X. Collard, J. Blin, A. Bensakhria, J. Valette, *Journal of Analytical and Applied Pyrolysis*, 95 (2012) 213.
11. S. Wang, W. Guo, K. Wang, Z. Luo, *Journal of Analytical and Applied Pyrolysis*, 91 (2011) 183.
12. J. Chang, Y. Fu, Z. Luo, *Biomass and Bioenergy*, 39 (2012) 67.
13. P. Lv, Z. Yuan, L. Ma, C. Wu, Y. Chen, J. Zhu, *Renewable Energy*, 32 (2007) 2173.
14. K. Salo, W. Mojtahedi, *Biomass and Bioenergy*, 15 (1998) 263.
15. B. Buragohain, P. Mahanta, V.S. Moholkar, *Energy*, 35 (2010) 2557.
16. Y. Zhang, B.L. Hongtao, B. Zhang, *Thermochimica Acta*, 538 (2012) 21.
17. C.R. Vitasari, M. Jurascik, K.J. Ptasinski, *Energy*, 36 (2011) 3825.
18. V. Strezov, M. Patterson, V. Zymla, K. Fisher, T.J. Evans, P.F. Nelson, *Journal of Analytical and Applied Pyrolysis*, 79 (2007) 91.
19. K.O. Lim, *Biomass and Bioenergy*, 4 (1993) 301.
20. M. Kumar, R.C. Gupta, T. Sharma, *Biomass and Bioenergy*, 3 (1992) 411.
21. J.A. Fuwape, *Bioresource Technology*, 57 (1996) 91.
22. T. Minowa, T. Kondo, S.T. Sudirjo, *Biomass and Bioenergy*, 14 (1998) 517.
23. S.S. Toor, L. Rosendahl, A. Rudolf, *Energy*, 36 (2011) 2328.
24. D.C. Elliot, E.G. Baker, D. Beckman, Y. Solantausta, V. Tolenthiemo, S.B. Gevert, C. Hornell, A. Ostman, B. Kjellstrom, *Biomass*, 22 (1990) 251.
25. A. Demirbas, *Energy Conversion and Management*, 41 (2000) 1601.
26. A.M. Radwan, H.A. Sebak, N.R. Mitry, E.A. El-Zanati, M.A. Hamad, *Biomass and Bioenergy*, 5 (1993) 495.
27. Y.H. Zheng, J.G. Wei, J. Li, S.F. Feng, Z.F. Li, G.M. Jiang, M. Lucas, G.L. Wu, T.Y. Ning, *Renewable and Sustainable Energy Reviews*, 16 (2012) 4588.
28. F.M. Hons, J.T. Cothren, J.C. Vincent, N.L. Erickson, *Biomass and Bioenergy*, 5 (1993) 289.
29. T.M. Sandip, C.K. Kanchan, H.B. Ashok, *Bioresource Technology*, 110 (2012) 10.
30. V.A. Malik, S.L. Lerner, D.L. MacLean, *Gas Separation & Purification*, 1 (1987) 77.
31. R. He, J. Wang, F.F. Xia, L.J. Mao, D.S. Shen, *Chemosphere*, 89 (2012) 672.
32. K. Takeshige, K. Ouchi, *Journal of Fermentation and Bioengineering*, 79 (1995) 11.
33. V.D. Nguyen, J. Auresenia, H. Kosuge, R.R. Tan, Y. Brondial, *Biochemical Engineering Journal*, 55 (2011) 208.
34. I.M. Atadashi, M.K. Aroua, A.R. Aziz, N.M. Sulaiman, *Renewable and Sustainable Energy Reviews*, 16 (2012) 3275.
35. E. Santacesaria, G.M. Vicente, M. Serio, R. Tesser, *Catalysis Today*, 195 (2012) 2.
36. L. Fryda, K.D. Panopoulos, E. Kakaras, *Energy Conversion and Management*, 49 (2008) 281.
37. A.O. Omosun, A. Bauen, N.P. Brandon, C.S. Adjiman, D. Hart, *Journal of Power Sources*, 131 (2004) 96.
38. D. Singh, E. Hernandez-Pacheco, P.N. Hutton, N. Patel, M.D. Mann, *Journal of Power Sources*, 142 (2005) 194.
39. M. Sucipta, S. Kimijima, K. Suzuki, *Journal of Power Sources*, 174 (2007) 124.
40. M. Santarelli, S. Barra, F. Sagnelli, P. Zitella, *Bioresouce Technology*, 123 (2012) 430.
41. C. Athanasiou, F. Coutelieris, E. Vakouftsi, V. Skoulou, E. Antonakou, G. Marnellos, A. Zabaniotou, *International Journal of Hydrogen Energy*, 32 (2007) 337.
42. R.C. Rady, S. Giddey, S.P. Badwal, B.P. Ladewig, S. Bhattacharya, *Energy & Fuels*, 26 (2012) 1471.

43. Y. Nabae, K. Pointon, J. Irvine, *Journal of the Electrochemical Society*, 156 (2009) B716.
44. S.Y. Ahn, S.Y. Eom, Y.H. Rhie, Y.M. Sung, C.E. Moon, G.M. Choi, D.J. Kim, *Applied Energy*, 105 (2013) 207.
45. H. Li, Q. Liu, Y. Li, *Electrochimica Acta*, 55 (2010) 1958.
46. X. Li, Z. Zhu, R. DeMarco, J. Bradley, A. Dicks, *Journal of Power Sources*, 195 (2012) 4051.
47. J.P. Kim, H.K. Choi, Y.J. Chang, C.H. Jeon, *International Journal of Hydrogen Energy*, 37 (2012) 11401.
48. G.A. Hackett, J.W. Zondlo, R. Svensson, *Journal of Power Sources*, 168 (2007) 111.
49. K. Xu, C. Chen, H. Liu, Y. Tian, X. Li, H. Yao, *International Journal of Hydrogen Energy*, 39 (2014) 17845.
50. R. Antunes, M. Skrzypkiewicz, *International Journal of Hydrogen Energy*, 40 (2015) 4357.
51. N. Kaklidis, V. Kyriakou, I. Garagounis, A. Arenillas, J.A. Menendez, G.E. Marnellos, M. Konsolakis, *RSC Advances*, 4 (2014) 18793.
52. O. D. Adeniyi, <http://etheses.whiterose.ac.uk/1964/> Last accessed 06/27/2013.
53. M. Dudek, R. Socha, *International Journal of Electrochemical Science*, 9 (2014) 7414.
54. A. Elleuch, K. Halouani, Y. Li, *Journal of Power Sources*, 281 (2015) 350.
55. A. Elleuch, A. Boussetta, J. Yu, K. Halouani, Y. Li, *International Journal of Hydrogen Energy*, 38 (2013) 16590.
56. J. Yu, Y. Zhao, Y. Li, *Journal of Power Sources*, 270 (2014) 312.
57. B. Cantero-Tubilla, C. Xu, K. Sabolsky, J.W. Zondlo, E.M. Sabolsky, *Journal of Power Sources*, 238 (2013) 226.
58. B. Timurkutluk, C. Timurkutluk, M.D. Mat, U. Kaplan, *International Journal of Energy Research*, 25 (2011) 1048.
59. Y.D. Zhen, A.I.Y. Tok, S.P. Jiang, F.C.Y. Boey, *Journal of Power Sources*, 178 (2008) 69.
60. S.C. Singhal, K. Eguchi, *Solid Oxide Fuel Cells 12 (SOFC-XII): ECS Transactions*, 35 (2011) 474.
61. P. Gansor, C. Xu, K. Sabolsky, J.W. Zondlo, E.M. Sabolsky, *Journal of Power Sources*, 198 (2012) 7.
62. D. Pantea, H. Darmstadt, S. Kaliaguine, L. Summchen, C. Roy, *Carbon*, 39 (2001) 1147.
63. C. Jiang, J. Irvine, *Journal of Power Sources*. 2011: 196: 7318-7322.
64. H.M. El-Nashaar, S.M. Griffith, J.J. Steiner, G.M. Banowetz, *Bioresource Technology*, 100 (2009) 3526.
65. G. Banowetz, S. Griffith, H.M. El-Nashaar, *Energy and Fuels*, 23 (2009) 502.
66. M. Mazarei, H. Al-Ahmad, M.R. Rudis, B.L. Joyce, N. Stewart, *Plant Science*, 181 (2011) 712.
67. Z.K. Trocsanyi, A.F. Fieldsend, D.D. Wolf, *Biomass and Bioenergy*, 33 (2009) 442.
68. H.M. El-Nashaar, G.M. Banowetz, S.M. Griffith, M.D. Casler, K.P. Vogel, *Bioresource Technology*, 100 (2009) 1809.